Optical bandgap modelling from the structural arrangement of carbon nanotubes

Butler, Timothy P; Rashid, Ijaz; Montelongo, Yunuen; Amaratunga, Gehan A J; Butt, Haider

DOI:
10.1039/c7nr09567h

Document Version
Peer reviewed version

Citation for published version (Harvard):
Butler, TP, Rashid, I, Montelongo, Y, Amaratunga, GAJ & Butt, H 2018, 'Optical bandgap modelling from the structural arrangement of carbon nanotubes', *Nanoscale*, vol. 10, no. 22, pp. 10683-10690. https://doi.org/10.1039/c7nr09567h

Optical bandgap modelling from the structural arrangement of carbon nanotubes

Butler, Timothy P; Rashid, Ijaz; Montelongo, Yunuen; Amaratunga, Gehan A J; Butt, Haider

DOI:
10.1039/c7nr09567h

Optical Bandgap Modelling from Structural Arrangement of Carbon Nanotubes

Timothy P. Butler[1*], *Ijaz Rashid*[2], *Yunuen Montelongo*[3], *Gehan A. J. Amaratunga*[1], *Haider Butt*[2*]

[1]Centre of Advanced Photonics and Electronics, Electrical Engineering Division, Engineering Department, University of Cambridge, Cambridge CB3 0FA, UK

[2]School of Engineering, University of Birmingham, Edgbaston, Birmingham, B15 2TT, United Kingdom

[3]Department of Chemistry, Imperial College London, South Kensington Campus, London, UK

[*]Correspondence: tim23x@gmail.com, h.butt@bham.ac.uk

Telephone: +44 121 4158623

Keywords: Carbon nanotubes, Scattering, Diffraction, Photonic structures, Photonic bandgap, Optical bandgap

Abstract

Optical bandgap properties of the VACNT array were probed through its interaction with white light, with the light reflected from the rotating arrays measured by a spectrometer. The precise deterministic control over the structure of vertically-aligned carbon nanotube arrays through electron beam lithography and well-controlled growth conditions brings with it the ability to produce exotic metamaterials over a relatively large area. The characterisation of the behaviour of these materials in the presence of light is a necessary first step toward application. Relatively large area array structures of high quality VACNTs were fabricated in square, hexagonal, circular and pseudorandom patterned arrays with length scales on the order of those of visible light for the purpose of investigating how they may be used to manipulate an impinging light beam. In order to investigate the optical properties of these arrays a set of measurement apparatus was designed which allowed accurate measurement of their optical bandgap characteristics. Patterned samples were rotated under the illuminating white light beam, revealing interesting optical bandgap results caused by the changing patterns and relative positions of the scatterers (VACNTs).

Introduction

~~The electrons in a plasma or free electron gas, when subject to an impulse, will undergo a shift in distribution density under the force of the impulse. The corresponding charge imbalance caused by the movement of electrons relative to heavier ions in the substance induces a restoring electrostatic force; the electrons, moving under the influence of this force, exchange potential for kinetic energy and hence oscillate at some characteristic plasma frequency [1]. Metals are reflective in the optical range of the electromagnetic spectrum, as their plasma frequency is in the ultraviolet range. Metamaterials are structures with subwavelength features relative to a periodic external stimulus such as electromagnetic or acoustic waves. Pendry *et al* [2] show that when a metamaterial of thin metallic wires is~~

~~manufactured the effective plasma frequency of the structure can be lowered from that of the bulk material by up to six orders of magnitude, allowing the cutoff frequency for reflection of electromagnetic waves by the metamaterial to fall within the optical range. The range of frequencies which are screened can be selected by engineering structural parameters of the material; finely dividing a bulk metal into thin wires brings surface plasmons into play whose plasma frequency depends on the diameter of the wire and the proximity of its neighbours. The metallic nature of the VACNT arrays designed for these experiments allow them to interact similarly with an impinging EM wave [2]. Modification of the parameters of the CNT arrays will alter the effective surface plasmon frequency of the metamaterials formed by the array, changing the frequency at which it will allow an electromagnetic signal to pass [3].~~

Dielectric metamaterials may also exhibit frequency-dependent behaviour. When the refractive index of a dielectric metamaterial is periodically modulated over a length scale comparable with that of the wavelengths of impinging electromagnetic radiation then that material may be referred to as a photonic crystal, after the work of Sajeev John and Eli Yablonovitch in 1987 [2, 3]. In such a metamaterial certain frequencies of EM radiation may be completely reflected, either at certain angles of incidence (partial photonic bandgap) or all angles of incidence (complete photonic bandgap). The optical band gap, like the electronic band gap, has its origin in Bragg reflection [4]. The periodicity of photonic crystals can be one, two or three dimensional with physical examples being a Bragg reflector, a silicon oxide substrate with periodically etched holes and the naturally occurring stone opal, respectively.

Photonic crystals are materials which, like semiconductor or other crystals, have a periodic variation in their structure. In crystals this variation is due to the arrangement of the atoms and their electronic shells and is of the order of 0.1nm; its effects may be seen in the

diffraction of X-rays or in the formation of the bandgap in semiconductors. Photonic crystals however are formed from a periodic variation in refractive index contrast on the scale of hundreds of nanometres, that of the wavelengths of light. Crystals have a discrete rather than a continuous translational symmetry; they are invariant over some multiple of a fixed length.

There are naturally occurring photonic crystals but, as with semiconductors, those which are of practical use are usually man-made. An instance of a one-dimensional photonic crystal is the Bragg reflector, a stack of layers of alternating refractive indices whose properties can be chosen to reflect a select range of frequencies and thus act as an optical band stop filter. A plane wave travelling through the layers will be scattered at each interface, and the forward and backward propagating waves will interfere to form standing waves within the crystal. A standing electromagnetic wave existing within the stack can, due to the symmetry of the unit cell, either have its nodes centred in the low or the high refractive index layers [5].

As the velocity of the wave in a high refractive index must be lower than that of the wave in a low refractive index a bandgap appears of an energy equal to that of the difference between the two velocities. In order to model such a field in a 1D layered structure the 1D Helmholtz equation is solved by the plane wave expansion method [6]. The boundary conditions are determined at each layer by considering the transmitted and reflected waves and their tangential electric field component. The amplitude of the incident wave defines the first boundary condition at the interface which the wave strikes and the final boundary condition is set by the lack of reflection after the final interface.

Results and Discussion

A set of procedures were developed utilising a sophisticated combination of nanoscale patterning with electron beam lithography, deposition of catalyst layers and subsequent growth of vertically aligned carbon nanotubes. The procedures were optimised to make the most efficient possible use of the Nanobeam system, as this system was in very high demand for the duration of this experimental work. Deposition equipment designed and built within the Department of Engineering was used throughout the development of the process for sputtering and PECVD. SEM was used to characterise the height and spacing of the VACNT arrays, and the electron micrographs produced were analysed with a combination of freely available software and scripts written in MATLAB. Figure 1(a-d) shows the SEM images of fabricated VACNT arrays generated in square, hexagonal, circular and pseudorandom patterns using the MATLAB script written specifically for the purpose.

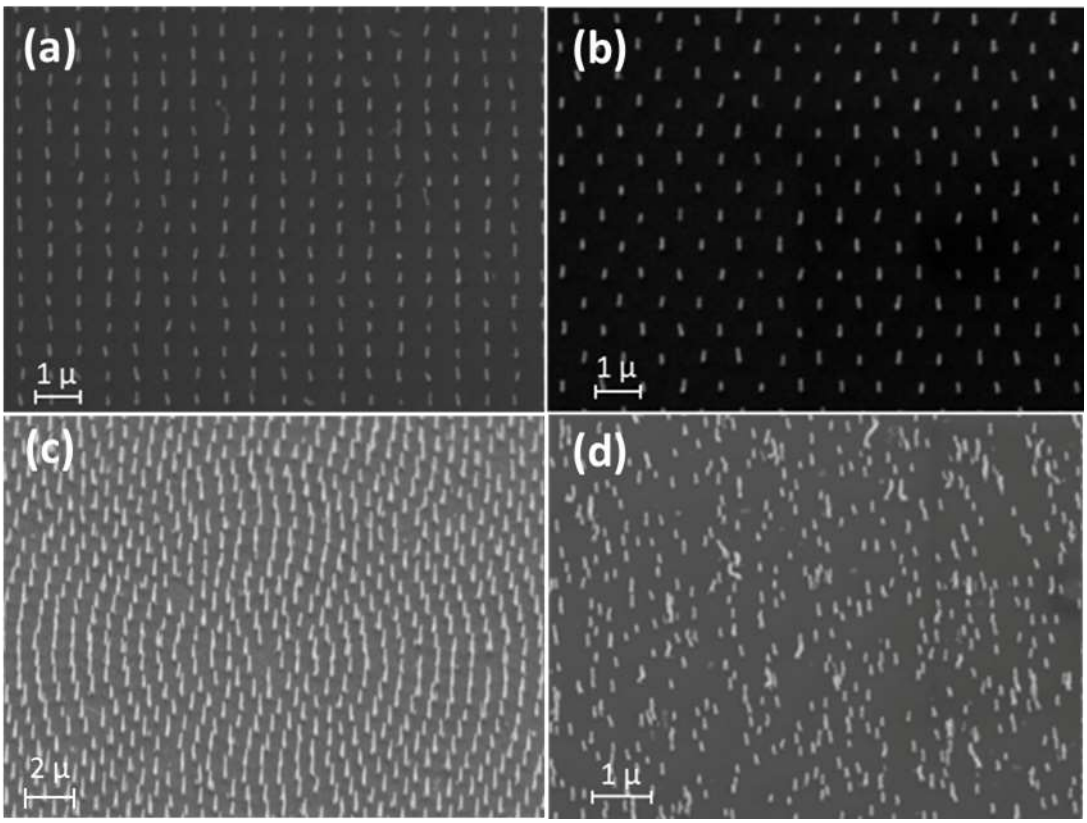

Figure 1: VACNT symmetry variation. (a) square, (b) hexagonal, (c) circular, (d) pseudorandom arrays of VACNTs

The effect of the arrays on white light were measured using a xenon lamp and a spectrometer [7]. To measure optical absorption, the xenon white light source is launched into a multimode optical fibre via a system of lenses mounted in a 30mm optical cage assembly attached to an optical bench. As the white light source for the measurement is a xenon lamp (Newport 6255, 150W), it should be switched on and allowed to stabilise for 30 mins before the start of experimentation [8]. The cage assembly allows the placement of filters before the launch lens to control the illumination level. The exit end of the fibre is mounted on an arm which allows adjustment of the angle of elevation. On exit from the fibre the light beam is collimated and polarised before impinging on the sample, and another arm-mounted fibre gathers the reflected light (Figure 2a). This fibre leads to an Ocean Optics HR2000 spectrometer. The sample is mounted on a rotation stage, driven by a computer controlled stepper motor. The sample is centred on the stage with the spectrometer in "live" mode. The initial angle of the sample is at zero degrees, i.e. an edge of the array is facing the light beam at the start of the experiment.

The collimated light beam forms an ellipse on the sample surface due to the angle of incidence. The receiving arm of the system, holding the fibre linked to the spectrometer, is adjusted to maximise the signal from the sample. A rapid, full rotation of the sample is carried out to check that the beam falls completely onto the array at the centre of the sample at all times, without hitting the bare silicon substrate. The level of signal at the spectrometer is checked to ensure that the spectrometer CCD is not saturating. If the signal saturates the CCD (> 4000 counts) then neutral density filters can be introduced into the light path to attenuate the beam before entering the fibre to the rig. After these checks, the stage is reset to zero. A baseline spectrum is recorded and the subsequent changes in transmission are recorded relative to this baseline. The angle of the sample is incremented by the required

amount and a spectral measurement taken. The rotation and measurement steps are repeated until the sample has undergone one full rotation.

To begin the experiment, the sample is rotated and a transmission spectrum gathered after each rotation step. CNT array samples of triangular and square symmetries with several different lengths were measured at various elevation angles. An angle step of 0.3 degrees was typically chosen, giving 1200 spectra of 2046 data points each per 360˚ rotation. The spectrometer has a wavelength range from 190 to 1100nm, giving a resolution of approximately 0.44nm per pixel. The full angular dependent transmission spectrum dataset thus consists of 2455200 data points, which was found to be presented in the most illuminating manner using a 2D greyscale image (Figure 2d) generated using a MATLAB script.

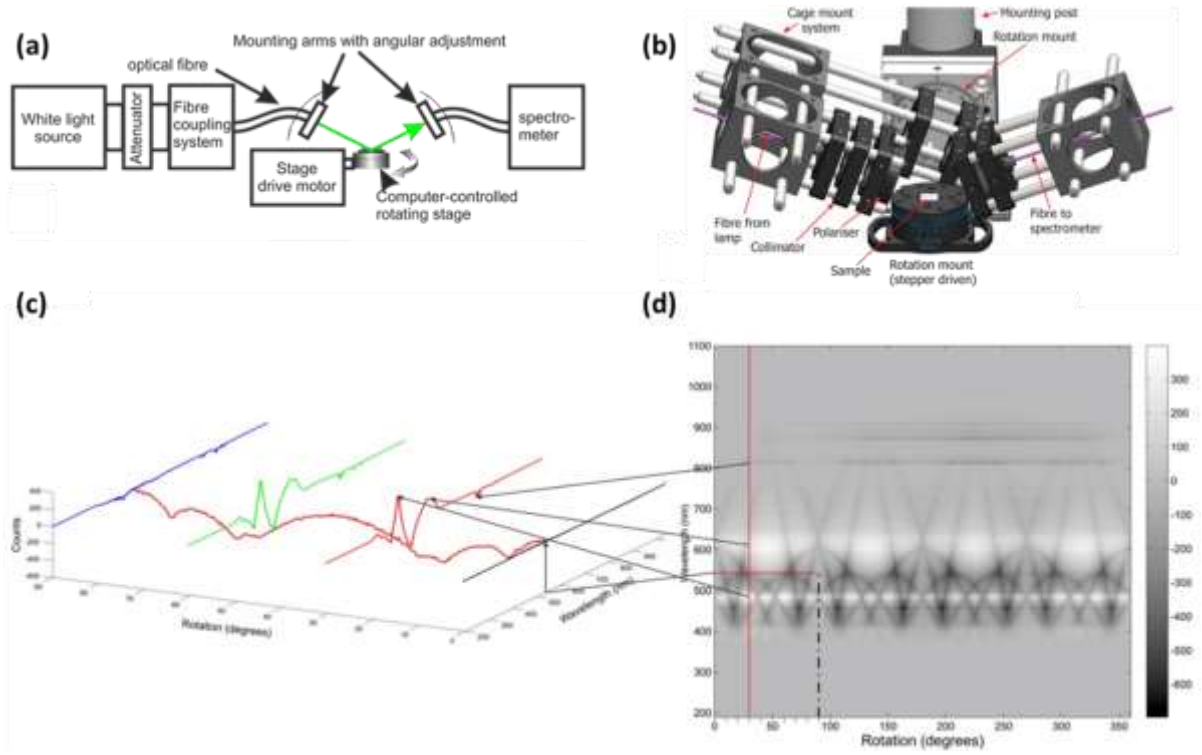

Figure 2: a) Diagram of transmission spectrum measurement system. b) CAD model of measurement system (some components omitted for clarity). The arms are individually

adjustable for elevation to allow for maximum signal. The stepper-driven rotation mount and spectrometer are under software control (LabVIEW). (c-d) Comparison of 3D plot vs. 2D intensity display for spectral absorption analysis, counts are represented by intensity, scaled to 256 bit greyscale. The positions of the red traces in the left panel are displayed as lines in the right, with some corresponding spectral features marked with arrows.

In **Error! Reference source not found.**2c the 3D plot contains a small subset of the data with spectra separated by 30˚; denser 3D plots tend to obscure spectral features. Therefore, in order to best present the results the whole experiment is converted into an intensity map. In the 2D intensity plot (**Error! Reference source not found.**2d) the individual spectra can be retrieved by taking the intensity profile along a vertical line with its base on the x-axis falling at the desired angle; for instance, the red traces in the 3D plot are obtained from the intensity profile of the red vertical line intersecting the x-axis at the 30˚ interval on the 2D image plot and the red horizontal line intersecting the Y axis at 538nm.

Transmission properties of square and hexagonal arrays were measured as described above. Figure 3a shows an SEM image of a typical square array of VACNTs respectively which were measured with the system. Each array measured was 2.5x2.5mm, to ensure that the light beam interacts entirely with the array. If the light beam impinges on the bare silicon substrate, the shape of the array becomes apparent in the 2D intensity map (Figure 3b-c).

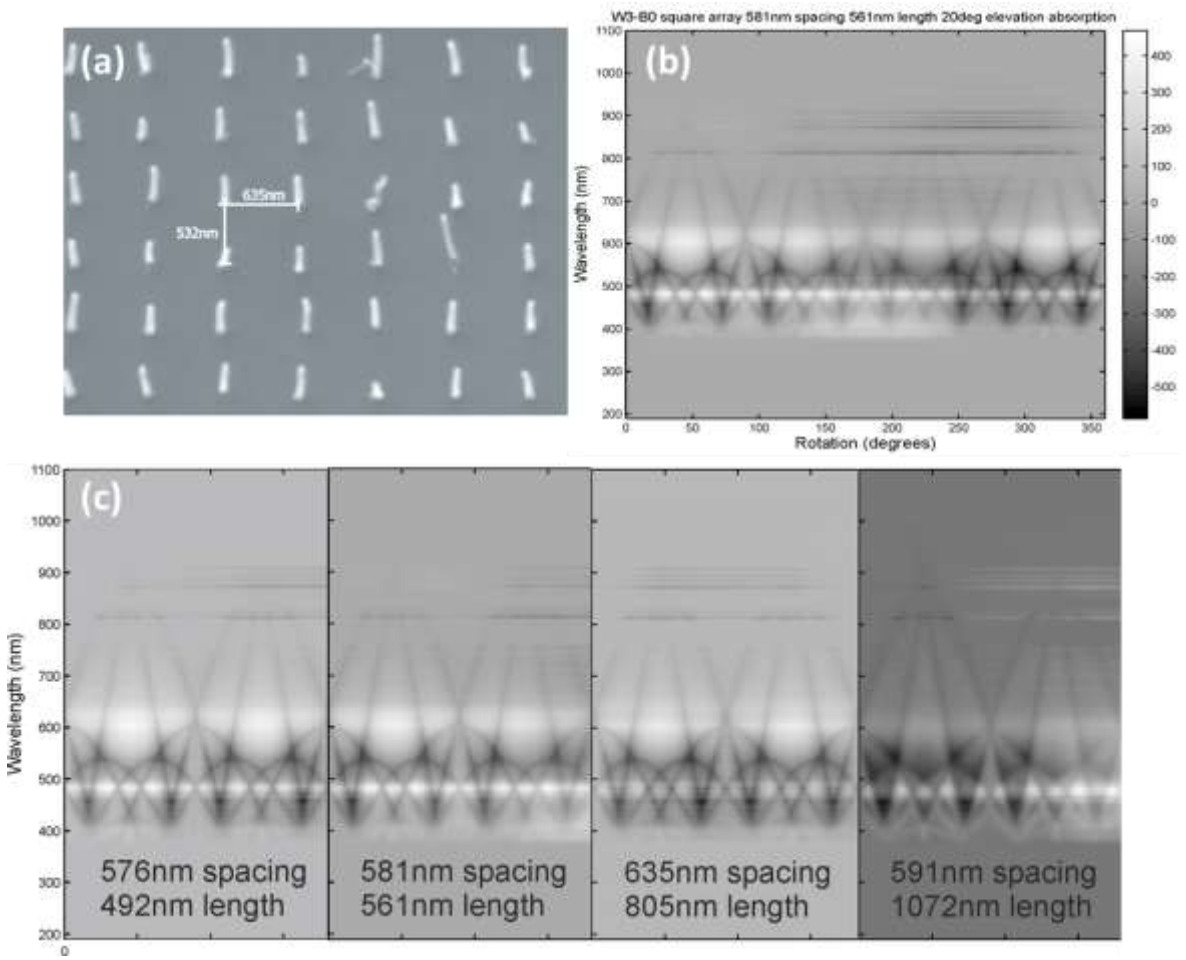

Figure 3: (a)Wafer 3 chip B0 – 635nm spaced square array, average tube length 561nm SEM image (tilt angle: 30 degrees), showing foreshortening along the y-axis due to the stage tilt. The azimuthal angle is zero degrees. (b) Transmission spectrum of a square VACNT array with 581nm spacing and 561nm length. The incident light beam is 70 degrees from normal. (c) Detail of transmission spectra for square arrays with varying apertures and VACNT lengths. Each detail section is a sample over 180°.

The rotation of the square array through 360° under illumination from white light results in an intensity map with a fourfold symmetry. The spectral emission of the illumination system (from about 400-900nm) limits the range in which the response of the array can be probed; the sensitivity of the spectrometer extends above and below this range. Reflected frequencies, failing to reach the spectrometer, appear as dark bands on the intensity map. Figure 4a-c shows an SEM image of a hexagonal array of VACNTs and the respective 2D intensity maps.

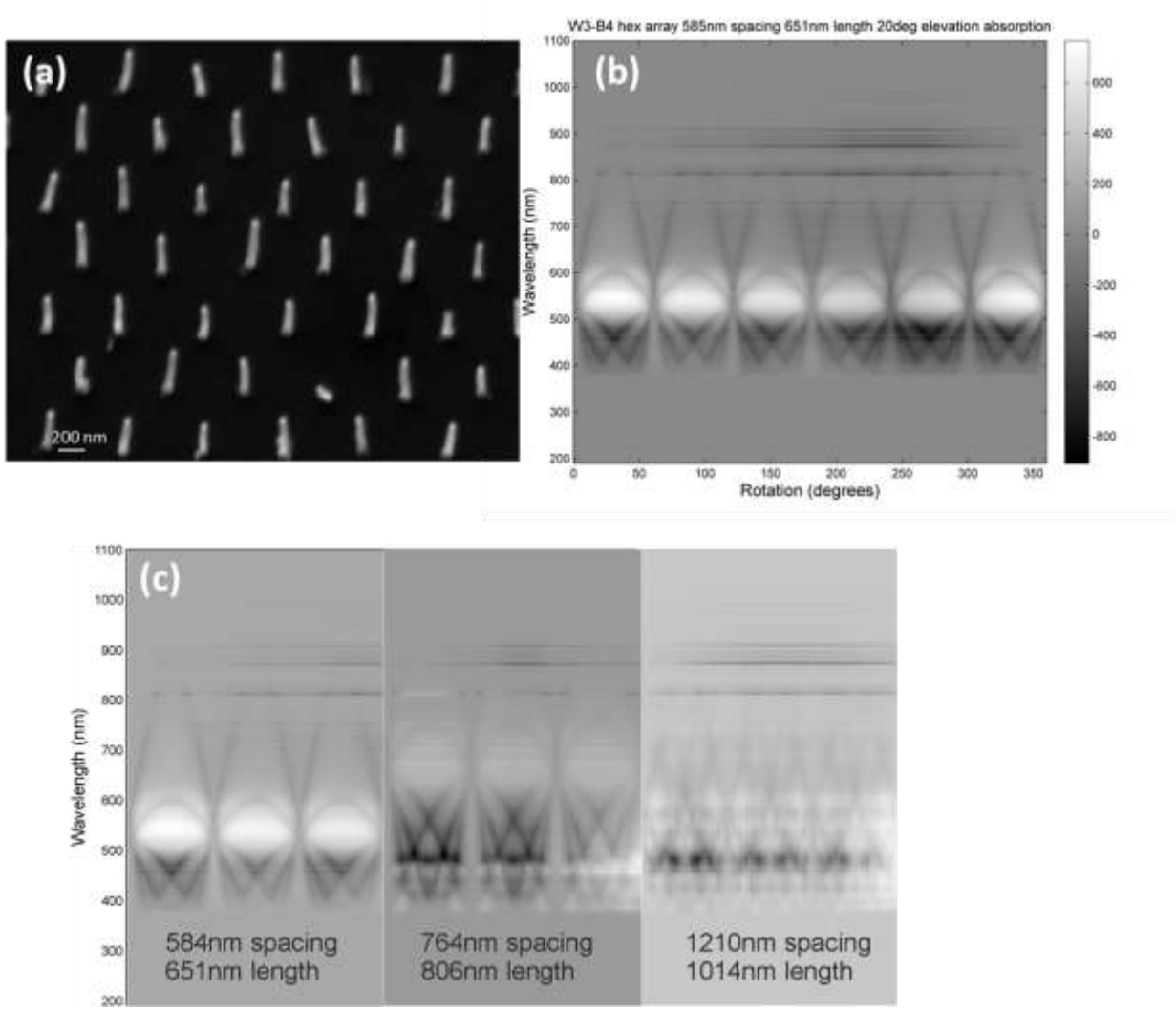

Figure 4: (a) SEM image of hexagonal arrays of VACNTs (b) Transmission spectrum of hexagonal VACNT array with 581nm spacing and 651nm length. The incident light beam is 70 degrees from normal. (c) Detail of transmission spectra for hexagonal arrays with varying apertures and VACNT lengths. Each detail section is a sample over 180°.

As the sample rotates, the reciprocal lattice rotates with it. In this way the wave vectors of the beam track through the Brillouin zone symmetry points and changes in the spectrum of light reflected from the sample will convey information about its optical band structure. The symmetries of the square and hexagonal arrays result in the respective fourfold and six fold replication of the transmission spectra in the intensity map which encompasses the full 360° revolution of the sample. The cosine patterns visible in the 2D map track the movement of

the frequency bands which are reflected by the array on the presentation of a particular configuration of scatterers to the incoming light beam. Looking in detail at the square array of sample W3-B0, cosine features with three distinct amplitudes can be seen (highlighted, (a, d) Detail of three transmission spectra from a square array with 4.5 degrees rotation difference. The top panel shows spectral measurement in wavelengths and counts, the bottom panel contains the corresponding section of the intensity map. 5a and 5d).

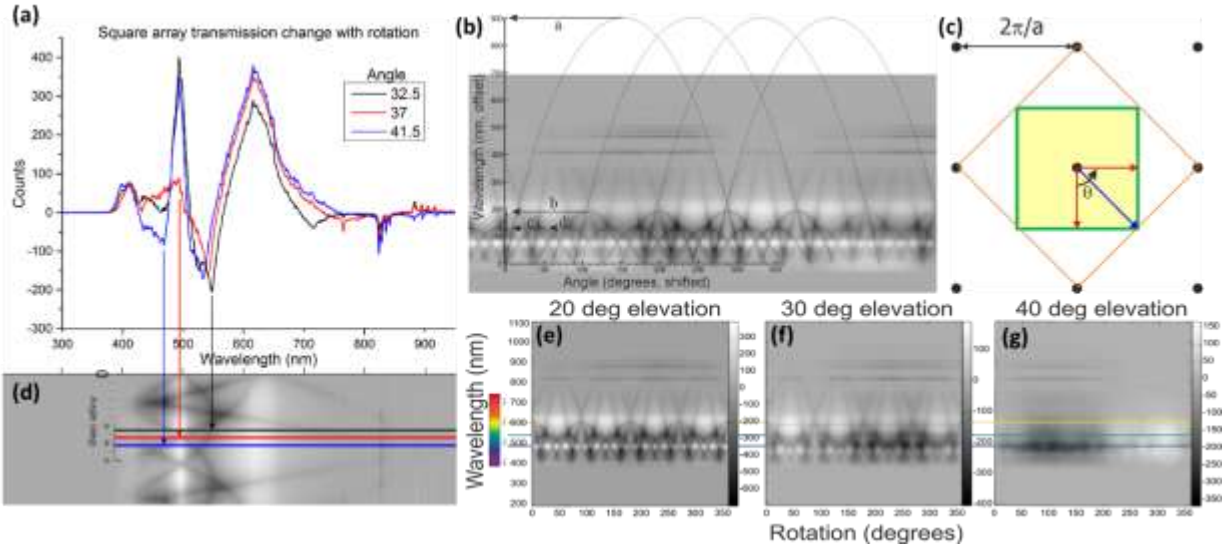

Figure 5: (a, d) Detail of three transmission spectra from a square array with 4.5 degrees rotation difference. The top panel shows spectral measurement in wavelengths and counts, the bottom panel contains the corresponding section of the intensity map. (b) Highlighted reflections from a square array of VACNTs. The transmission intensity map has been duplicated to simulate a 4π rotation of the sample. (c) Rotating the sample rotates the Brillouin zone (thick green square). The wave vector reflected by the first Brillouin zone increases in magnitude between 0 and 45 degrees, decreasing again from 45 to its original value at 90 degrees. (e-g) Sample W3-F4, square array with 576nm CNT spacing and 492nm length. The source and detector angle from the plane of the sample is increased from left to right.

The amplitude of the features is measured in nanometres, the phase and period in degrees.

Feature	Amplitude	Period	Phase

	(nm)	(degrees)	(degrees)
a	900	610	0
b	190	180	60
c	120	180	0
d	120	180	35

Table 1: Square array reflection cosine features

Sample W3-B0 is a square array with VACNTs spaced at 581nm; this is the aperture, a. The reciprocal lattice spacing is $\frac{2\pi}{a} = \mathbf{1.08^7 m^{-1}}$. As sample and hence the Brillouin zone rotates the scattering face of the Brillouin zone shifts. As the sample rotates up to 45°, gradually higher frequencies are reflected.

The sharp spectral features visible in the square and hexagonal arrays as the sample is rotated have their greatest contrast in the intensity maps when the light beam is as close as possible to the plane of the substrate on which the arrays are grown. The interaction of the light beam with the array would theoretically be at a maximum at zero degrees (cosine dependence); however, the short length of the VACNTs would present extreme challenges for coupling the light into the array. The dimensions of the measurement system limit the angle to a minimum of 20°. The spectral features are seen to diminish as the elevation angle is increased away from the plane of the substrate; the peaks of the features are virtually indistinguishable from the background at an elevation of 40 degrees.

As the angle of elevation is increased, the interaction of the light beam with the VACNTs decreases. When the beam is normal to the array, no band structure effects will be seen as the array is rotated as it becomes effectively homogeneous to the beam path. Diffraction of the beam will still be observed.

Changing the angle of the probe beam relative to the array will produce a change in the wave vector of the beam. This should produce a shift in the reflected frequencies. This shift is

visible between the spectra taken at 20˚ and 30˚, however the lack of interaction at 40˚ elevation makes it impossible to accurately determine the degree of shift. Table 2 details the measured shifts for two of the reflection peaks. As the elevation angle is increased, the peak reflection shifts to shorter wavelengths, i.e. longer wavelengths can now be transmitted through the array. Increasing the angle of elevation effectively increases the array spacing in the direction in which the light is travelling, which reduces the reciprocal lattice spacing and therefore the Brillouin zone. This reduction allows the transmission of the longer wavelengths.

Elevation (deg)	Rotation (deg)	Peak λ (nm)	shift (deg)
20	90	606	
30	90	587	-19
20	63	538	
30	63	527.5	-10.5

Table 2: Shift in peak absorption with elevation angle

Circular and pseudorandom arrays (Figure 6c top and bottom) were measured as systems with no symmetry. The pseudorandom array shows some variation in intensity as the array is rotated, but this is a broadband shift which may be explained by a slight tilt of the sample or stage causing a variation in the amount of light falling upon the spectrometer input. The circular array shows two bands of light, one centred around ~460nm and the other around ~480nm. The frequency of the band does not vary as the array is rotated, as would be expected from the array's circularity. On close inspection some slight banding can be seen; this is caused by the slight phase difference between the annular rings of the array. An interesting feature of this intensity map is the lack of oscillation seen at long wavelengths in all other measurements, between 800nm and 900nm. This array seems to be capable of uniform scattering except within the bluish bands of light previously mentioned.

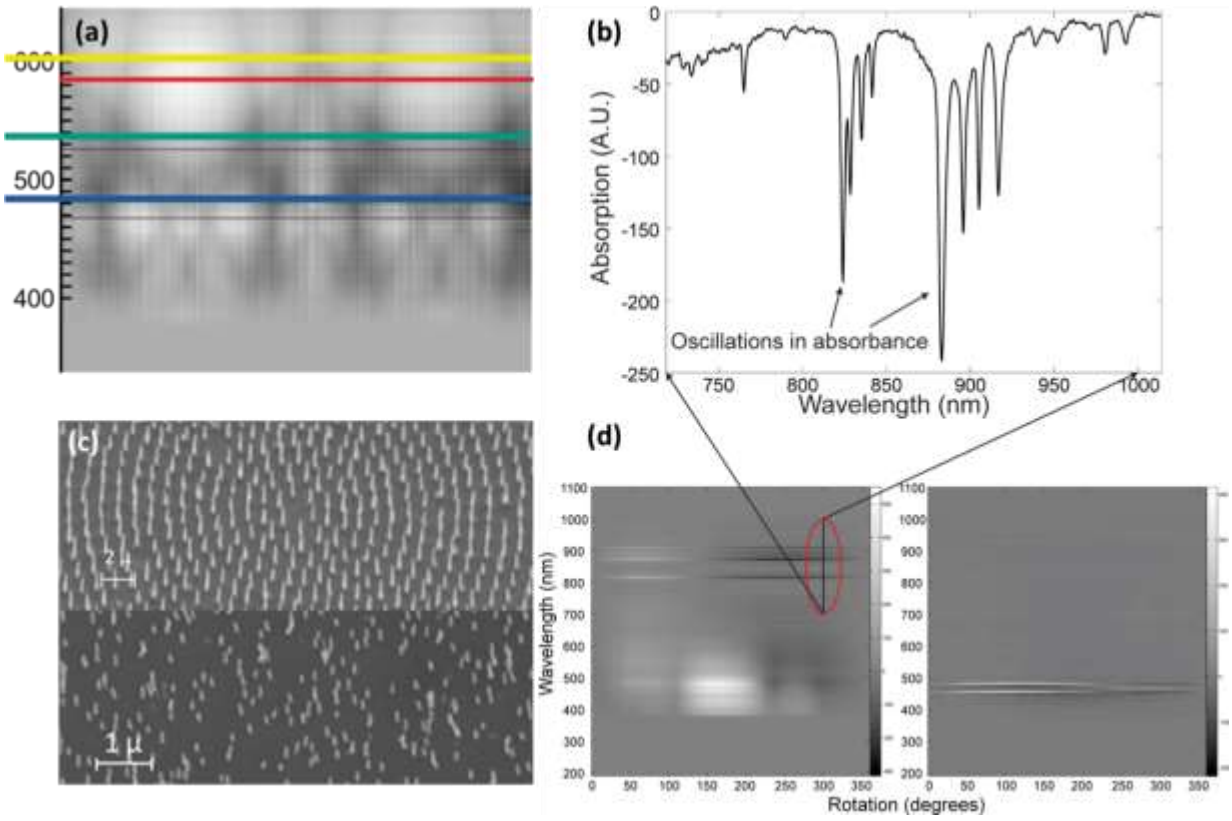

Figure 6: (a) Detail of square sample optical band structure measurement. The yellow line shows the peak of a cosine feature measured at 20 degrees elevation; the red line shows the new position of the peak when the measurement is carried out at an elevation of 30 degrees. The peak has shifted downward by approximately 19nm. (c) SEM image of Circular (top) and pseudorandom arrays (bottom) (d) Optical band structure measurements for pseudorandom (left panel) and circular VACNT arrays (right panel). Note the lack of banding between 800 and 900nm in the case of the circular array spectral map, detailed in the graph above (b)

The rotation of the array around its centre presents a changing view of the nanotube elements depending on the spacing and symmetry of the array. Each nanotube in the array describes an arc around the centre of rotation, with the arc described dependent upon the distance from the centre, r (the arc radius) and the angle through which the array is rotated in radians. Taken from the centre, the movement for a nanotube is θr for a rotation through θ degrees. Taking the example of the square array, at the initial azimuthal angle of 0˚ with the light beam impinging at an angle of 30˚ from the normal the array is presented as shown in the above

SEM image (Figure 3a). Increasing the tilt angle increases the apparent length of the tubes whilst foreshortening the apparent distance along the plane perpendicular to that of the tilt. This will increase the interaction of the light with the nanotubes and decrease the interaction with (reflection from) the substrate (Figure 7).

As the angle of incidence of the light beam deviates from the normal the interaction with the nanotube array will increase (Figure 7b). This allows a more accurate measurement of the bandgap as the signal to noise ratio (SNR) increases (Figure 5e-g). In this figure the decrease in contrast as the elevation angle from the plane of the substrate is increased in figures from left to right is clear. The square symmetry of the array is evident in the 90˚ periodicity of the scan features. As the angle is increased there is a slight decrease in wavelength of the absorption peaks, for instance that seen at an angle of 90˚.

MATLAB was used to model the periodic arrays of vertically-aligned carbon nanotubes as Bragg scatterers. A square array of scatterers is modelled in MATLAB. A vector, *v*, holds a range of values centred around zero. The MATLAB function REPMAT is used to duplicate the vector to produce a 2D array of x co-ordinates, which is then transposed to produce the corresponding array of y-co-ordinates for each scatterer in the square array. The angle and distance of each co-ordinate point from the centre is calculated. The Bragg condition for diffraction is calculated for each point for each angle of rotation of the array. As the array is square it exhibits fourfold symmetry so $\pi/2$ rotation captures the complete range of optical interaction.

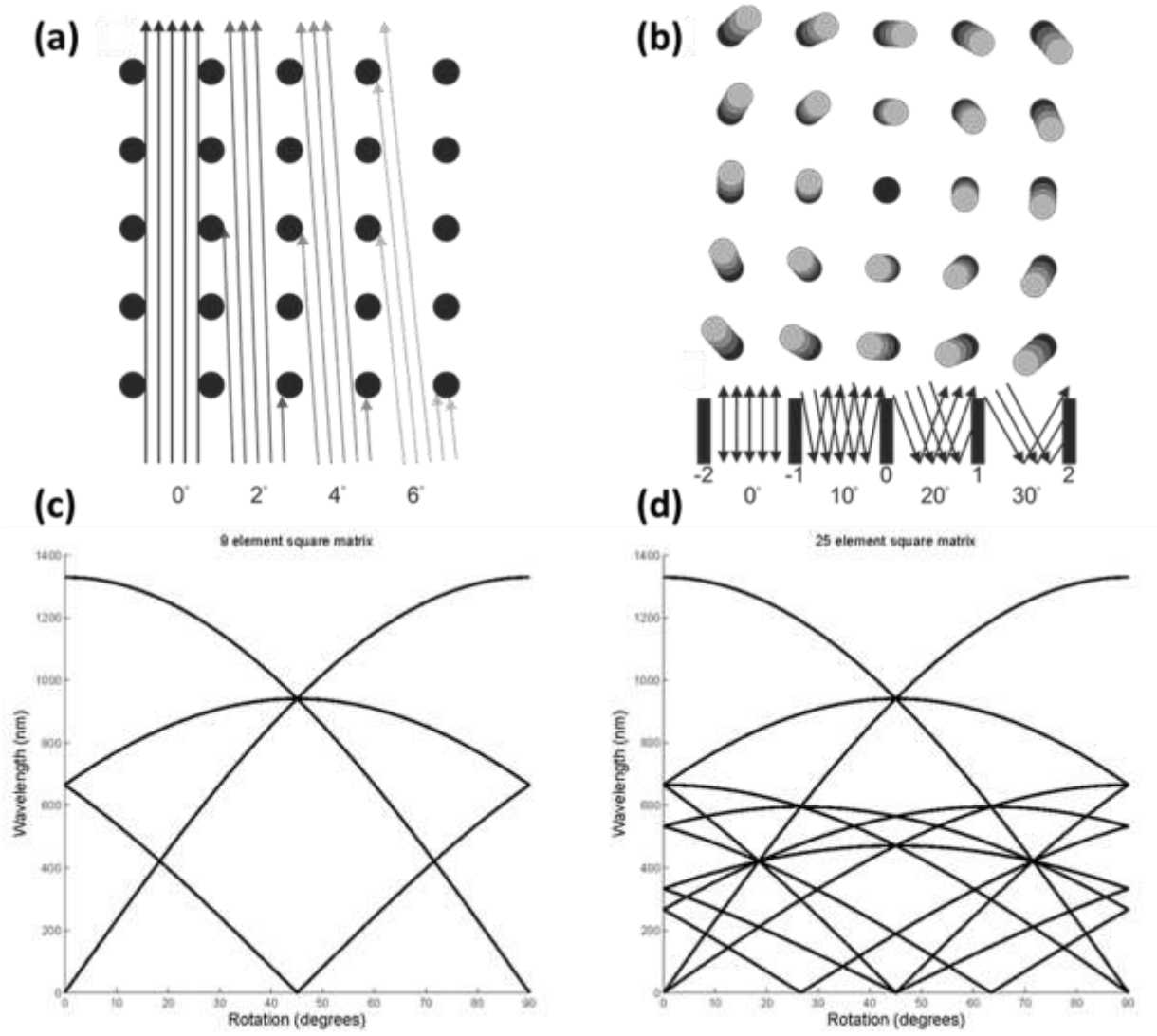

Figure 7: (a)Interaction of light beams with nanotube arrays at several azimuthal angles (b) shows a plan view of the rotating array (top) Light interaction at several elevation angles (bottom) (c,d) Comparison of optical band structure complexity when number of scatterers in a square array is increased from 9 (left panel) to 25.

Figure 7c-d shows plots of the optical band structure of the array of scatterers, as calculated from the Bragg law for reflection. The diagram shows that there are no complete band gaps, which would be indicated by discontinuities in the curves; i.e. there is no wavelength which is always scattered independent of the angle of rotation of the array.

Conclusions

The white light transmission measurements performed on square and hexagonal arrays of VACNTs demonstrate partial bandgaps in the optical regime. Complete bandgaps might be seen when probing the arrays with longer wavelengths. The Brillouin zone of the VACNT crystal was clearly evident in the cosine structures which follow troughs in the transmission of the probing white light beam. The circular array pattern showed a broadband, uniform scattering action. The two pass bands which were visible in the transmission spectrum could be moved by altering the growth parameters of the array. The combination of precision placing of VACNTs over a large area, high scattering cross section and highly tunable length suggests that there may well be applications for these structures in optical devices such as filters, switches and pumps. The limit on VACNT spacing for uniform growth with the processes used at present is 400nm. Complete photonic bandgaps may be realized with these symmetries by decreasing the ratio of aperture: wavelength either by reducing the spacing of the VACNTs or increasing the wavelength of light used. The broadband, uniform scattering of the circular array as measured in transmission can be further investigated through the generation of circular arrays with varied parameters of inter-ring spacing and phase. It should also be possible to tune the flat pass bands by varying these parameters. Square arrays may exhibit optical bandgaps at wavelengths longer than those in the visible spectrum. Measurements should be carried out using a light source whose emission and spectrometer sensitivity extends further into the micrometer range. The automation of the transmission measurement system, together with the grazing angle of incidence of the probe light beam made possible by the large areas of the arrays under scrutiny, have allowed the acquisition of high resolution optical transmission datasets. The mapping of these datasets clearly show the characteristic cosine curves of optical band structure which follows the rotation of the Brillouin zone with the sample. Square and hexagonal arrays show these curves following four and sixfold symmetry. Changing the grazing angle of incidence alters the effective shape

of the reciprocal lattice of the sample under test, with a corresponding change in the shape of the Brillouin zone. This change is evident in the lowering in amplitude of the cosine peak, which indicates longer wavelengths of light finding paths through the crystal structure. The circular array provides further interesting data. Apart from the two bands visible in the transmission map, extremely uniform broadband scattering has been achieved. This property is well deserving of further attention; circular array co-ordinates with greater spacings and phases between concentric rings are easily generated with the same software which created the original array.

Methods

Laboratory facilities at the Centre for Advanced Photonics and Electronics (CAPE) are used to fabricate relatively large area arrays of VACNTs of high quality with length scales on the order of those of visible light for the purpose of investigating how they may be used to manipulate an impinging light beam. In order to investigate the optical properties of these arrays, a set of measurement apparatus was designed which allowed accurate measurement of their various characteristics. The automation of the optical band structure measurements produced a very high resolution map of the energies reflected and transmitted by the arrays as they were rotated under the illuminating white light beam, revealing interesting structures caused by the changing relative positions of the scatterers. The interaction of light with the array was qualitatively reproduced with a MATLAB model.

The second system was based around optical cage components purchased from Thorlabs and used to measure optical bandgap effects by directing white light onto the array and measuring the reflected spectrum. Both of these systems had measurement interfaces written in LabVIEW, allowing a higher volume of accurate data to be recorded than would have been possible with manual measurements and therefore increasing the quality of the dataset used in later analysis. The large, accurate datasets produced became particularly useful in the optical

bandgap measurements. A step by step summary of sample preparation and characterization process is provided in the supporting material.

Acknowledgements

References

1 R. P. Feynman, R. B. Leighton, M. Sands, and E. M. Hafner, The Feynman Lectures on Physics, vol. 1, 3 vols. Addison-Wesley, 1963.

2 J. B. Pendry, A. J. Holden, W. J. Stewart, and I. Youngs, "Extremely Low Frequency Plasmons in Metallic Mesostructures," Phys. Rev. Lett., vol. 76, no. 25, p. 4773, Jun. 1996.

3 H. Butt, Q. Dai, P. Farah, T. Butler, T. D. Wilkinson, J. J. Baumberg, and G. A. J. Amaratunga, "Metamaterial high pass filter based on periodic wire arrays of multiwalled carbon nanotubes," Appl. Phys. Lett., vol. 97, no. 16, p. 163102, 2010.

4 C. Kittel, Introduction to Solid State Physics, 8th Edition. John Wiley & Sons, 2004.

5 J. D. Joannopoulos, S. G. Johnson, J. N. Winn, and R. D. Meade, Photonic Crystals: Molding the Flow of Light, 2nd Revised edition. Princeton University Press, 2008.

6 I. A. Sukhoivanov and I. V. Guryev, Photonic Crystals: Physics and Practical Modeling. Springer, 2009.

7 W. M. Robertson, G. Arjavalingam, R. D. Meade, K. D. Brommer, A. M. Rappe, and J. D.Joannopoulos, "Measurement of photonic band structure in a two-dimensional periodic dielectric array," *Phys. Rev. Lett.*, vol. 68, no. 13, pp. 2023–2026, Mar. 1992.

8 V. Astratov, "Photonic band-structure effects in the reflectivity of periodically patterned waveguides," *Phys. Rev. B*, vol. 60, no. 24, pp. R16255–R16258, 1999.Han, Z. *et al.* Active Antifogging Property of Monolayer SiO2 Film with Bioinspired Multiscale Hierarchical Pagoda Structures. *ACS nano* **10**, 8591-8602 (2016).